Link to Leeds Beckett Repository record:
http://eprints.leedsbeckett.ac.uk/5191/

Document Version:
Article

PV with multiple storage as function of geolocation

Giuseppe Colantuono*, Ah-Lian Kor, Colin Pattinson, Chris Gorse

Leeds Sustainability Institute, Leeds Beckett University, LS1 3HE Leeds, UK

Abstract

A real PV array combined with two storage solutions (**B**, battery, and H, hydrogen reservoir with electrolyzer-fuel cells) is modeled in two geolocations: Oxford, UK, and San Diego, California. All systems meet the same 1-year, real domestic demand. Systems are first configured as standalone (SA) and then as Grid-connected (GC), receiving 50% of the yearly-integrated demand. H and PV are dynamically sized as function of geolocation, battery size B_M and H round-trip efficiency η_H.

For a reference system with battery capacity $B_M = 10$ kWh and $\eta_H = 0.4$, the required H capacity (B_M) in the SA case is ~1230 kWh in Oxford and ~750 kWh in San Diego (respectively, ~830 kWh and ~600 kWh in the GC case). Related array sizes are 93% and 51% of the reference 8 kW$_\text{p}$ system (51% and 28% for GC systems). A trade-off between PV size and battery capacity exists: the former grows significantly as the latter shrinks below 10 kWh, while is insensitive for B_M rising above it. Such a capacity achieves timescales' separation: **B**, costly and efficient, is mainly used for frequent transactions (daily periodicity or less); cheap, inefficient H for seasonal storage instead.

With current PV and **B** costs, the SA reference system in San Diego can stay within $2 \cdot 10^4$ \$ CapEx if H's cost CapEx(H_M) does not exceed ~7 \$/kWh; this figure increases to 15 \$/kWh with Grid constantly/randomly supplying a half of yearly energy (4 \$/kWh in Oxford, where no SA system is found below $2 \cdot 10^4$ \$ CapEx).

Rescaling San Diego's array (further from its optimal configuration than Oxford's) to the ratio between local, global horizontal irradiance (GHI) and Oxford GHI, yields in all cases a 11% reduction of size and corresponding cost, with the other model outputs unaffected. The location dependent results vary to different extents when extending the modeled timeframe to 18 years. In any case, the variability stays within $\pm 10\%$ of the reference year.

Keywords: energy meteorology; peak demand; photovoltaics; seasonal/ intraday electricity storage; grid integration

---

*Corresponding author, colantuono@gmail.com

1. Introduction

Non-constant output is a major obstacle towards a widespread exploitation of wind and solar photovoltaic (PV) generation (Boyle, 2012; Steinke et al., 2013; Aghaei and Alizadeh, 2013; Denholm et al., 2015); energy storage is widely seen (Section 2) as the necessary addition for both the integration of large fractions of renewable electricity into the power Grid as well as the local utilization. Storage on the users' side can also free the Grid from the need of following demand. The price of batteries was still relatively high at the beginning of the 2010s (Mulder et al., 2013; Juul, 2012) but has then started to decline sharply; by some analysts (Hensley et al., 2012), this decreasing trend is projected to continue.

PV power is a typical example of highly inconstant renewable generation. Time-variability of solar irradiance on the Earth surface is due to the planet's rotation and revolution, which in turn correspond to separated timescales: day-night and seasonal cycles. The third source of irregularity is due to weather and climate, and is superimposed to the deterministic astronomical oscillations. It is termed intermittency in renewables literature and has a prominent effect on PV output, particularly in cloudy regions (see for example Colantuono et al., 2014a). Storage coupled to PV power must cope with these three sources of variance. The growing field of research of Energy meteorology (Emeis, 2012; Kleissl, 2013; Olsson, 1994) testifies the importance of environmental analysis for maximizing renewables' output and quantifying/reducing uncertainty (Correia et al., 2017; Prasad et al., 2015; Colantuono et al., 2014b). Several authors have suggested to combine various storage technologies to respond to such diverse timescales (e.g. Zhou et al., 2011; Glavin et al., 2008). Studies coupling batteries and hydrogen storage are reviewed in Section 2. Here, the same domestic load (this choice is explained in Section 4.4) in two geographical locations is considered: Oxford, UK, and San Diego, California. Firstly, demand is satisfied by PV (defined by the installed peak power) as the only power source, integrated with two coexisting storage reservoirs, schematized by their efficiency and cost: a long term hydrogen reservoir, H, coupled to electrolyzer and fuel cells, and a short term battery $\mathbf{B}$. Capacity of H, H_M, and PV array's size are dynamically determined for the chosen locations by two requirements: demand at every time must be met, and the yearly-integrated value of demand must equal the yearly-integrated value of generation, after conversion inefficiencies have been taken into account. PV output and states of charge of the storage reservoirs are expressed as function of time in both geolocations. PV size is expressed by means of the scaling factor X, the fraction of the 8 kW$_\mathrm{p}$ array used as reference (Appendix A). The partition of storage into a long-term reservoir and a short-term, more efficient and smaller one is justified if a trade-off between storage cost and conversion inefficiency is possible.

Current storage technologies possess various efficiency levels; here, hydrogen H and battery $\mathbf{B}$ are characterized by their round-trip efficiency values η_H and η_B. H efficiency is given three values: $\eta_H = 30\%$, 40% and 50%, a range similar to what reported in Luo et al. (2015, Table 11 therein), while the

battery efficiency is fixed at $\eta_B = 85\%$ (*ibid.*). The latter value can fall either within the lithium-ion (Rastler, 2010) or the lead-acid (Beaudin et al., 2010) efficiency interval. The smallest η_H value is the closest to the currently available electrolysis/fuel-cell cycle; significant improvements may be expected with standardization and mass production, as hydrogen storage is still in the development phase (Luo et al., 2015). Engineering implementation is, however, beyond the scope of this analysis, the focus of which is energy balance. Environmental temperature is likely to impact round-trip efficiency of storage but would be difficult to define, as it depends not only on external temperature but also on buildings' features, placement of reservoirs within the property, resulting heat exchange with the environment, etc. The ample efficiency range we posit for H is comprehensive of any potential effect, included the high uncertainty on the performance that commercially-ready seasonal storage systems will achieve.

PV generation is then supplemented by a Power Grid able to provide only constant power. This scenario explores storage as a substitute of the current load-following pattern (e.g. Moshövel et al., 2015); the amount of long- and short-term storage needed on the user's side to accommodate such a constant supply is quantified. This idea is further extended that a partly random power provision is fed by utilities to domestic customers, to understand how users' storage may cope with a Grid that, besides not following demand, does not mitigate the variability on the supply side induced, for example, by wind and solar farms.

A simple CapEx analysis is then carried out, with the goal of comparing costs as system configurations vary in different geolocations. Such estimates provide a clue about the financial penalty potentially imposed, across different Earth regions, by seasonal storage (and its combination with other system's components), the cost of which is highly uncertain. Finally, a long-term (18 yr) irradiance analysis is performed in both locations, to show how local irradiance variability differs from place to place, and what this implies for system sizing.

The main goal here is to highlight geographical/climate differences, and the behavior induced by various battery sizes. The sizing of a real system would have to account, for example, for year-to-year differences in solar generation and electricity consumption, failure rate, and other unpredictable factors; consequently, some form of uncertainty evaluation should be introduced, e.g. loss-of-load probability (LOLP, discussed by Celik, 2007; Klein and Beckman, 1987; Schenk et al., 1984, and many others). The impact of differences in PV generation over many years is addressed in Section 7, as well as the effect of varying demand. LOLP or similar metrics are not estimated here, as this would not make substantial contribution to frame the problem of multiple storage as function of climate and geolocation.

2. Literature Review

Analyses carried out so far about sizing/performance of battery-hydrogen hybrid storage (BHHS) systems is reviewed in this Section. In very few cases a

comparison between different geolocations has been attempted in the past: extant BHHS literature focuses on engineering implementation, control strategies and dispatching rules rather than the environment. Irradiance variability beyond the "typical year" assumption of commercial energy models is scarcely, if ever, addressed. The recent paper of Zhang et al. (2017) points out the unsuitability of batteries and the advantages of hydrogen storage (high energy density and negligible leakage rate) to address irradiance seasonal imbalance affecting PV generation. They locate the imbalance in "Nordic countries"; imbalance is however significant everywhere on Earth, midlatitudes and tropics included. Scamman et al. (2015) compare the behavior of PV with BHHS in two geolocations: Heraklyon (with wind generation also present), Greece, and Phoenix, Arizona; this paper recognizes (as, from a different perspective, Cebulla et al. 2017) the importance of evaluating the behavior of a combination of load, generation and hybrid storage across different climates (performance in Reykjavik, Iceland, is also examined, with electricity entirely generated by a wind turbine). The case study therein considers a constant, 1 kW load; the authors conclude that their BHHS off-Grid system reduces the need for battery capacity, prolonging also battery life; a typical year of solar irradiance in each location is estimated using a commercial model. Marchenko and Solomin (2017) uses real irradiance data for an off-Grid system close to Lake Baikal, Russia; irradiance is measured during a time interval of 2 weeks per season and then extended using historical trends. Zhou et al. (2008) size a stand-alone BHHS and a geolocation comparison is carried out, dealing with modeled, 1-yr irradiance; the foci of the paper are system's engineering and dispatching rules. A similar comment may be made about Jacob et al. (2018). Advancing technology, rather than exploring the effects of environmental conditions, is also the prevalent interest of Cau et al. (2014); Maclay et al. (2007); Li et al. (2009); Jallouli and Krichen (2012); Kolhe et al. (2003); Gomez et al. (2009). Ulleberg (2004) mainly addresses control strategies for PV-hydrogen systems, while an island Grid with battery and seasonal storage is the subject of Brinkhaus et al. (2011). The island is simulated in a generic location with a given battery size; the whole system is managed by a programmable logic controller to direct power into either the battery or hydrogen storage. Controlling algorithms for hybrid storage in a single location are the focus of Bigdeli (2015) and Gabrielli et al. (2017), while the system's rules in Tesfahunegn et al. (2011) minimize degradation.

3. Summary of Contribution

The comparison of physical, biological and engineering systems' behavior in different environments and climates is of prominent relevance in many fields of science and engineering (Rotter et al., 2012; Lam et al., 2008; Gholz et al., 2000; Running and Nemani, 1988, among many possible high-impact studies), particularly when some kind of resource varies with the system's position on the Earth surface, as is the case of solar irradiance. The BHHS standalone (SA)

Table 1: Main symbols

Symbol	Definition
$\mathcal{S}\,()$	Heaviside's step function
$T = 1$ year	Length of the problem in time
$0 \equiv t_0, t_1, ...t_n, ..., t_N \equiv T/t_1$	60 s time-steps; $N = T/60s \equiv 525600$
d^B	Power from battery to load in kW
d^H	Power from H to battery in kW
u^B	Power from generation to battery in kW
u^H	Power from generation to H in kW
λ	Electric power load in kW
γ	PV power generation in kW
δ	Difference between generation and demand in kW
X	Fraction of the reference, 8 kW$_p$ PV array
$\mathbf{B}$ and $\mathcal{B}$	Battery and its state of charge in kWh
H and $\mathcal{H}$	Hydrogen storage and its state of charge in kWh
η_H	Energy efficiency of long term storage (H)
η_B	Efficiency of short term storage (battery)
B_m	Minimum battery charge level in kW
B_M	Battery capacity in kWh

system with PV (the "System" from now on) is sized under the condition of yearly-integrated generation matching consumption ("balance") with conversion penalties taken into account. Real generation and irradiance are used, enabling the estimation of required seasonal storage capacity H_M as System's position varies on Earth surface. The year-to-year uncertainty affecting H_M is estimated. The "intensity of usage" of seasonal storage is strongly location-dependent and is quantified by the "roughness parameter" r, a novel non-dimensional number here introduced for the first time. Comparing geolocations in this context enables estimation of the weight of System's components, their relevant parameters and mutual interactions on System's behavior. System's configurations are analyzed in the parameter space by varying battery capacity B_M and seasonal storage efficiency η_H, which cause changes in H_M and X in order to preserve balance. Extension of the analysis to the GC case explores two unusual types of power provision: Grid power, either constant or partly random, *must* be received and stored if not immediately used. Finally, a cost analysis determines the sensitivity of system CapEx to physical parameters and components' cost.

4. Modeling the System

4.1. Generalities

The examined System comprises a 1 year-long domestic load from central France (Appendix A Lichman, 2013) where the climate, loosely speaking, is somehow intermediate between the analyzed locations. Load is then scaled to set

its yearly-integrated value to 5 MWh. PV generation needs to be standardized accordingly: its yearly-integrated value in both locations must equal 5 MWh to match demand *after the losses due to storage round-trip conversions are taken into account*. This implies that changing **B** reservoir's size makes PV array's area and H's capacity, H_M, changing as well. Further case studies include power provision from the electric Grid in the amount of 50% of the yearly-integrated demand, with PV array's size reduced accordingly. A System with no battery (endowed with H only) has not been considered due to the relatively slow start-up time of fuel cells. As soon as battery is discharged below $X \cdot \max(\lambda) \cdot 600$ s, d^H, the supply from seasonal storage H, is triggered. A 600 s interval is of the order of H's reservoir latency (without entering in details about fuel-cell technologies, the 10 minutes value of Qi, 2013, page 184, is here chosen as a safe estimate). Such a buffer makes effective **B** capacity, B_M, lower than labeled. In a real System, an additional small penalty, neglected here, would be present, because a fraction of the power drawn from H would be routed through **B** in transient phases, before H reaches working conditions (Lacko et al., 2014). The number of transients would be small, as H is accessed with a much lower frequency with respect to **B**.

4.2. Governing equations

We are aimed at determining storage reservoirs' states of charge $\mathcal{B}(t_n)$ and $H(t_n)$ as function of previous states $\mathcal{B}(t_{n-1})$ and $H(t_{n-1})$ and of generation $X\gamma$ and load λ. X needs to be determined as well. Time dependency is henceforth omitted to simplify notation, barring cases where functions depend on previous time step t_{n-1}.

We first define δ, the difference between generation and load at any time t_n:

$$\delta = X \cdot \gamma - \lambda \, ; \tag{1}$$

X scales the generation timeseries γ to adapt PV array's nominal power to System's features as they are varied throughout the model's scenarios.

We then label uploaded and downloaded power as u^B, u^H, and d^B, d^H. Power flows are defined ≥ 0: they are subtracted from the reservoir/node (Fig. 1) they leave, while they are added to the reservoir/node they reach. Variables u^B and u^H quantify the power uploaded to battery **B** and to long-term reservoir H, respectively:

$$
\begin{aligned}
u^B ={}& \tilde{\mathcal{S}}[\, B_M - \eta_B \delta - \mathcal{B}(t_{n-1})] \cdot \mathcal{S}(\delta) \cdot \delta + \\
&+ \mathcal{S}\big\{ -[\, B_M - \eta_B \delta - \mathcal{B}(t_{n-1})] \big\} \cdot [\, B_M - \mathcal{B}(t_{n-1})] / \eta_B \,,
\end{aligned} \tag{2}
$$

$$
u^H = \mathcal{S}\big\{ -[\, B_M - \eta_B \delta - \mathcal{B}(t_{n-1})] \big\} \cdot \big\{ \delta + [\mathcal{B}(t_{n-1}) - B_M] / \eta_B \big\} \, ; \tag{3}
$$

symbols are detailed in Table 1, while

$$
\mathcal{S}(x) = \begin{cases} 1, & \text{if } x > 0 \, ; \\ 0, & \text{otherwise} \, ; \end{cases} \quad \text{and} \quad \tilde{\mathcal{S}}(x) = \begin{cases} 1, & \text{if } x \geq 0 \, ; \\ 0, & \text{otherwise} \, ; \end{cases}
$$

6

is the Heaviside's step function, according to either the $\mathcal{S}(0)=0$ or the $\tilde{\mathcal{S}}(0)=1$ convention (brackets of any kind following $\mathcal{S}$ always denote its functional argument). This function plays the role of a switch, defining the System's regime: for example, when δ changes from positive to negative, the quantity $\tilde{\mathcal{S}}(\delta)$ goes from 1 to zero, setting the first term of Eq. (2) to zero. This is all the more so for the second term (and for the right-hand side of Eq. 3 as well), because $\delta \leq 0$ implies $\eta_B \cdot \delta + \mathcal{B}(t_{n-1}) - B_M \leq 0$.

Battery is being charged ($u^B > 0$) when both generation is larger than λ (that is, $\delta > 0$) and $\mathbf{B}$ is not full; if either condition is not met, $u^B = 0$ holds instead. On the other hand, long-term storage H is being charged ($u^H > 0$) when $\delta > 0$ and $\mathbf{B}$ is completely filled up; that is, the relationships $\mathcal{B}(t_n - 1) = B_M$ and $X \cdot \gamma > \lambda$ are true at the same time. The first term of Eq. (2) represents the case in which the 60 s "energy packet" to be loaded at the current time-step does not saturate the capacity of the battery when added to the energy already in it. The second term refers to the incoming packet saturating the battery, in which case the packet can only be partially taken up. In the latter instance, the energy uploaded to $\mathbf{B}$ corresponds to the difference between capacity B_M and $\mathcal{B}(t_n - 1)$, the level of charge resulting from balance at previous time-step. The energy needed to fill such a capacity is the capacity itself divided by $\mathbf{B}$'s efficiency $\eta_B < 1$; this takes into account round-trip storage losses, for simplicity attributed entirely to the uploading phase. The only term on the right-hand side of Eq. (3) "completes" the action of the second term of Eq. (2): the fraction of the incoming energy packet that does not fit in $\mathbf{B}$ (or the entire packet, if $\mathcal{B}(t_{n-1}) = B_M$) is uploaded to H instead.

Power downloaded *from* reservoirs is instead denoted by the non-negative functions d^B and d^H:

$$d^B = -\mathcal{S}(-\delta) \cdot \delta ; \tag{4}$$
$$d^H = -\mathcal{S}(-\delta) \cdot \mathcal{S}[B_m - \mathcal{B}(t_{n-1})] \cdot \delta ; \tag{5}$$

In order for d^B to be greater than zero (that is, for battery to discharge) the condition $\delta < 0$ is sufficient. This is due to the fact that, in the model, d^H is computed as "in transit" through the battery (see Eq. 6 below) before being delivered to the demand side. In the physical world, the battery would be bypassed by the energy delivered by H in order not to incur in the efficiency penalty η_H; to take this requirement into account, the d^H term appears with coefficient 1 in the H balance (Eq. 6) and is denoted by a unique line-style in the System's diagram (Fig. 1). Besides the condition on δ, d^H must also meet $\mathcal{B}(t_{n-1}) < B_m$: the discharge of energy from H to the demand side is triggered when the battery level falls below threshold B_m. Battery level is restored at $\mathcal{B} = B_m$ or higher as soon as δ becomes greater than zero. Until that occurs, H remains active; that is, d^H remains above zero.

We can finally quantify the energy level in both $\mathbf{B}$ and H reservoirs:

$$\mathcal{B} = \mathcal{S}(t_2 - t_n) \cdot B_M + \mathcal{S}(t_n - t_1) \cdot \left\{ \mathcal{B}(t_{n-1}) + \eta_B u^B + d^H - d^B \right\} ; \tag{6}$$
$$\mathcal{H} = \mathcal{S}(t_2 - t_n) \cdot \mathcal{H}(0) + \mathcal{S}(t_n - t_1) \cdot \left[\mathcal{H}(t_{n-1}) + \eta_H u^H - d^H \right] ; \tag{7}$$
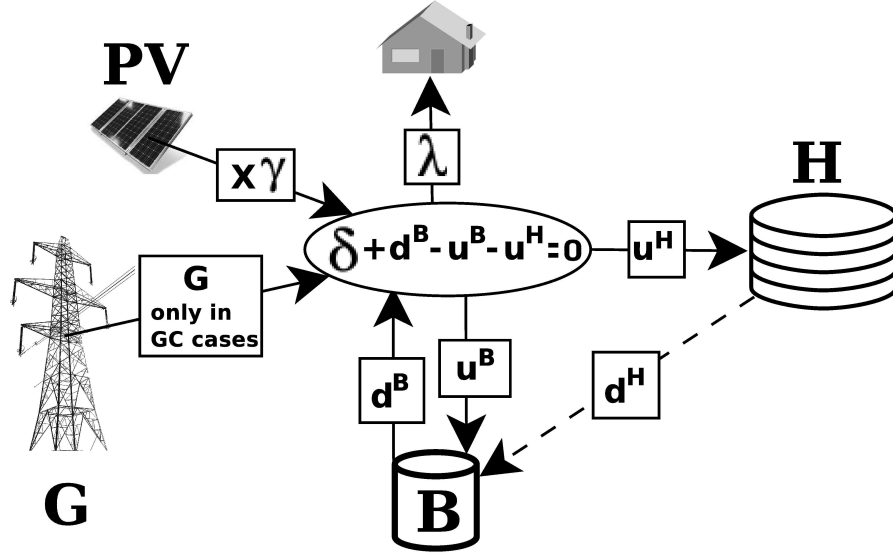
7

Figure 1: Diagram for the analyzed System. H and **B** denote the reservoirs, as in the main text. "PV" indicates the PV array, "G" the Power Grid, when present, while the house icon symbolizes the demand side. δ is defined either by Eq. (1) or by Eq. (12), depending on the System being Grid-connected or not. The ellipse represents an idealized node where all incoming/outgoing power contributions sum up to zero. Arrows indicate the flowing power and its direction; all quantities are positive. d^B, d^H, u^B, and u^H are defined by Eqs. (2-5). d^H is triggered by both $\delta < 0$ and battery charge falling below B_m; however, it flows through the battery without being subject to the η_B penalty and without altering the battery state of charge, hence the dashed arrow. In a real System, d^H could be simply routed from H reservoir to the node.

Heaviside's conditions, in this case, separate reservoirs' initial energy level ($t_n = 1$) from the evolution that follows ($t_n > 1$).

In summary, both $\mathcal{B}$ and $\mathcal{H}$ depend on load λ and generation $X\gamma$ via δ through Eqs. (2-4); $\mathcal{B}$ and $\mathcal{H}$ also depend on time, on the fixed parameters B_m, B_M, η_B, η_H, and on their prior states. Examples of the behavior of the seven variables defined by Eqs. (1-7) are displayed in Appendix B.

The last equation needed to close the problem is given by the constraint

$$\mathcal{H}(T) + \mathcal{B}(T) = \mathcal{H}(0) + B_M ; \tag{8}$$

i.e., it is required that the final amount of stored energy equals the initial level (the System starts with full battery, $\mathcal{B}(0) \equiv B_M$): this assures that yearly-integrated generation and load are equal as well, once all conversion's inefficiencies have been taken into account. In order to find a practical, approximate solution, the equality in Eq. (8) will be considered satisfied if the two sides differ less than a predetermined amount ("error").

Uploading to the less efficient, long-term reservoir only when battery is full minimizes the required PV array's size (or, equivalently, energy usage); it has

also the advantage of not requiring any kind of online computation. Once **B**'s capacity B_M is fixed and both H and the PV array are sized accordingly, the historical data (past generation and demand timeseries) will not be necessary for operating a real System.

4.3. Solution of Eqs (1-8)

Equations are solved for every time t_n as function of previous time t_{n-1}, for a guessed value of X; the procedure is being iterated until "error" falls below a predetermined threshold. $X = 1$ corresponds to a PV installation with exactly the size of the 8 kW$_p$reference array; the model can be thought to start every time with such a guess, which affects the computational time only. H at $t = 0$ contains an amount of energy equal to 2 months of the yearly-integrated load: $\mathcal{H}(0) = (5/6)$ MWh (the used datasets are detailed in the next section). The first step (from 00:00 to 00:01, January 1) simply updates battery storage, which is depleted by a value corresponding to 60 s worth of load as PV generation is zero at nighttime. As time advances, the appropriate Heaviside's functions will transit from zero to 1 and vice versa. **B** becomes progressively depleted, but the Sun later kicks in. **B** may therefore be recharged or, if generation is insufficient, may fall below the minimum level B_m, in which case H will start to feed the demand instead. At the end of the yearly timeseries, the final value $\mathcal{H}(T) + \mathcal{B}(T)$ is recorded.

For the sake of computing a practical solution, Eq.(8) is replaced by the following approximate condition, as anticipated above:

$$| \mathcal{H}(T) + \mathcal{B}(T) - \mathcal{H}(0) - B_M | < 10 \text{ kWh} . \tag{9}$$

If Eq. (9) is not satisfied and the argument of the absolute value on the left-hand side is negative, the size of the PV array is increased by means of increasing X; if, on the contrary, such an argument is positive, X will be reduced. After this update the procedure is repeated and $\mathcal{H}$ updated again. The process is interrupted as soon as the condition in Eq. (9) is met. Capacity of long-term storage H is defined as

$$H_M = \max [\mathcal{H}(t_n)] - \min [\mathcal{H}(t_n)] . \tag{10}$$

The 10 kWh allowed maximum difference (error) between initial and final $\mathcal{H}$ value is here considered negligible with respect to the 5 MWh yearly-integrated load. The model allows to arbitrarily reduce the error, at expense of computational speed. From the coding point of view, a "while loop" is being employed to keep the model running and the iterations following one another until an appropriate PV array's size is found and the inequality at Eq. (9) satisfied. When this occurs, yearly generation balances the yearly demand, storage's round-trip penalties included.

DA QUI

4.4. Demand and Generation data

A domestic consumption timeseries and a PV generation one are needed in each geolocation. The same domestic-load (Lichman, 2013) is used in both localities: Oxford, UK (hereafter Oxford, Oxford PV array 2016) and San Diego, CA, USA (San Diego from now on, PVOutput.org 2017b). This choice has the downside of neglecting the local correlation between PV generation and household power demand (e.g., on a sunnier-than-average day, lower lighting demand may be expected, together with relatively high PV output) but has the advantage of comparing performance of both generation and storage in different locations against *the same* demand curve, which is the main goal of this study. With the loss of co-spatiality between generation and demand, contemporaneity loses its meaning, too: timeseries have been therefore chosen to prioritize availability and data integrity.

Load λ is normalized to 5 MWh of yearly generation, which cuts approximately by a half the integrated value of the original timeseries (Appendix A). 5 MWh is considerably lower than the electrified USA home's yearly consumption ($\sim$ 12300 kWh in 2014, Energy Efficiency Indicators 2016) but higher than the average home in the European Union ($\sim$ 3600 kWh, *ibid.*) and in China ($\sim$ 1600 kWh).

The array size needed in San Diego is 61% of Oxford's one to achieve the same yearly-integrated output (Eq. A.1) for the available generation timeseries. This introduces a dependency on the particular year considered when comparing the two geolocations. In Section 7, 18-year long records of global horizontal irradiance (GHI) are considered, to overcome this limitation and determine a range of variability for the model's quantities. The size of PV arrays is expressed in kW_p, to keep conclusions independent from the technology used. The fact that arrays' orientation is not identical (Appendix A) is also worth a comment. The ratio between the just mentioned, time-integrated 18-years GHI in Oxford and San Diego is 0.54, to be compared to the generation ratio value, 0.61 (Eq. A.1). A possible, alternative approach (not free from drawbacks, as discussed at the bottom of Section 7) could be the rescaling of every San Diego's size factor X by $0.54/0.61 = 89\%$. We here limit the analysis to the comparison between the available real Systems. This said, differences induced by Systems' configuration (battery size, H efficiency, Grid supply) are assessed by comparing results locally.

5. Results

5.1. Standalone Systems

Standalone Systems are useful analysis targets not only per se; they can be viewed as the limiting case for Grid-connected (GC) Systems, with PV and storage, as Grid-supplied electricity is progressively reduced. Eqs. (6-8) are solved for $\mathcal{B}$, $\mathcal{H}$, and X thirty times for each location, in order to combine three values of η_H (0.3, 0.4, 0.5) with ten values of battery size B_M (2 to 20 kWh with 2 kWh increment). Solutions are sought by dynamically adjusting X such that

$X \cdot \gamma$ satisfies the demand λ (Appendix A) for the chosen battery size within the specified, 10 kWh error.
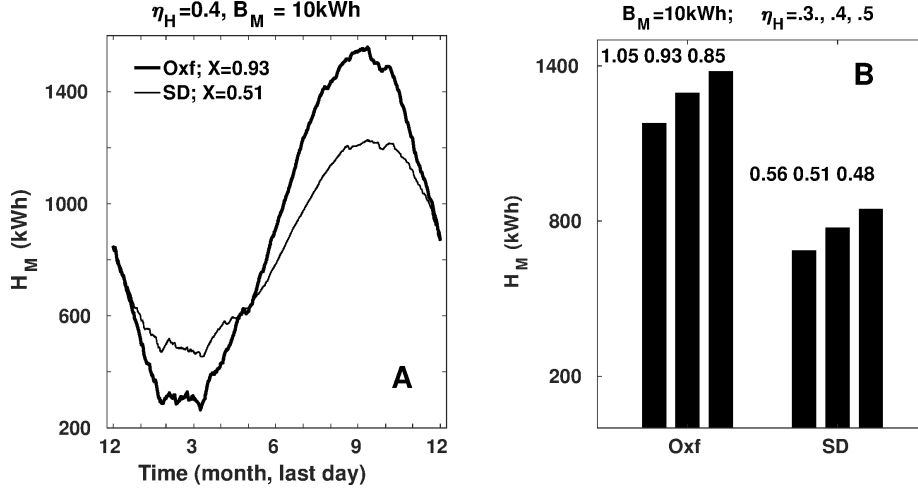

Figure 2: Panel **A**. Curves represent $\mathcal{H}$ throughout the year in the two geolocations for the specified η_H and B_M values. The $\mathcal{H}$ curve in Oxford (San Diego) boasts higher (lower) maxima and lower (higher) minima: more energy must be stored in Spring/Summer (Summer from now on) to be used in Fall/Winter (hereafter Winter) in more poleward latitudes. Panel **B**. H capacity as function of H's round-trip efficiency $\eta_H = 0.3, 0.4, 0.5$ (corresponding to 1st, 2nd, and 3rd bar for each geolocation). The numbers at the top of each bar portrait X, the PV array scaling factor; a similar scaling applies if PV's area is considered instead of peak power, provided technology is the same for all Systems.

Figure 2A depicts the effect of geolocation on required hydrogen storage capacity, defined as the difference between maximum and minimum amount of energy contained in the H reservoir. Figure 2B portraits required H_M and PV size as function of hydrogen conversion efficiency in each location. Demand can be satisfied in Oxford by a PV array with size between 85% and 105% of the 8 kW_p reference installed power, for a power-to-hydrogen round-trip conversion efficiency η_H between 30% and 50% and a 10 kWh battery. The same conditions in San Diego require an array ranging from 48% to 56% of the 8 kW_p reference power. The required PV size decreases with increasing η_H because a more efficient H storage reduces conversion losses and, consequently, the generation required to meet demand. Conversely, the required H_M capacity grows as a smaller PV array will increase the Fall/Winter energy deficit. In other terms, with a larger PV array and a less efficient seasonal storage H, more power is proportionally wasted in Summer to load the hydrogen reservoir (it is useful to recall that round-trip inefficiencies are here computed at once when energy is uploaded to reservoirs) but less energy is actually uploaded, as the larger array is closer to self-sufficiency in Winter.

Fig. 3A's curves depict PV size requirement as function of battery size B_M once the intermediate hydrogen conversion efficiency has been picked ($\eta_H = 0.4$). They highlight that increasing battery size from $\mathcal{B} = 10$ kWh to $\mathcal{B} = 20$ kWh
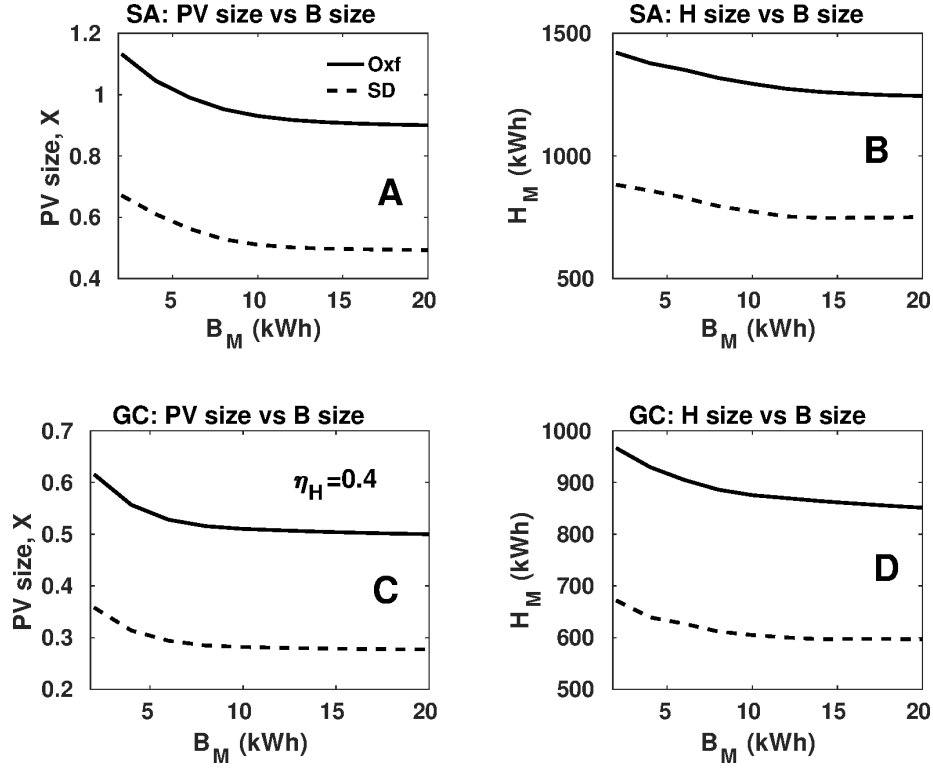
Figure 3: H_M and PV size variations with respect to battery size, for both standalone and Grid-connected Systems. Panels **A** and **C** suggest 10 kWh as the appropriate battery size for the given load. Increasing B_M beyond 10 kWh does not significantly reduce the required PV size/generation. H_M follows a similar, even if weaker, law in the two higher-latitude locations. Legends in Panels **A**, **C** refer to all plots.

offers only marginal PV reduction: the required PV size reaches an "asymptotic" (or, at least, as such definabe for practical purposes) value in each location, corresponding to the day-night cycle being completely satisfied by batteries. On the other hand, the difference between the PV size required for a 10 kWh and a 2 kWh battery is significant because, when B_M is too small, the System is forced to rely on relatively inefficient H storage for hourly and daily transactions which occur with high frequency, from hundreds to a few thousands of times per year, compared to the few cycles per year (1 or 2) involved in seasonal storage. The difference in the PV array size required by $\mathcal{B}=2$ kWh and $\mathcal{B}\geq 10$ kWh suggests that the separation between long-term (seasonal) and short-term (daily-hourly) storage arises in a seamless and "natural" way when battery is large enough. No energy-management algorithm is required to direct power to the appropriate reservoir: the simple rule of first filling **B** up to capacity, and only subsequently converting electricity to hydrogen and loading the H reservoir, has the property of minimizing conversion inefficiencies and therefore minimizing the PV area

required to feed the System.

Figure 3B shows the effect battery size has on required H capacity, qualitatively similar in Oxford and San Diego. A smaller battery (which, as already seen, implies a larger PV array) increases H_M as the energy lost in Fall/Winter using inefficient H for day-night transactions is made up for by extra energy stored during Summer. We may also notice, as a secondary effect, that day-night transactions at the end of Summer, when H stores the maximum amount of energy, imposes a few extra kWh of capacity to compensate for the smaller battery.
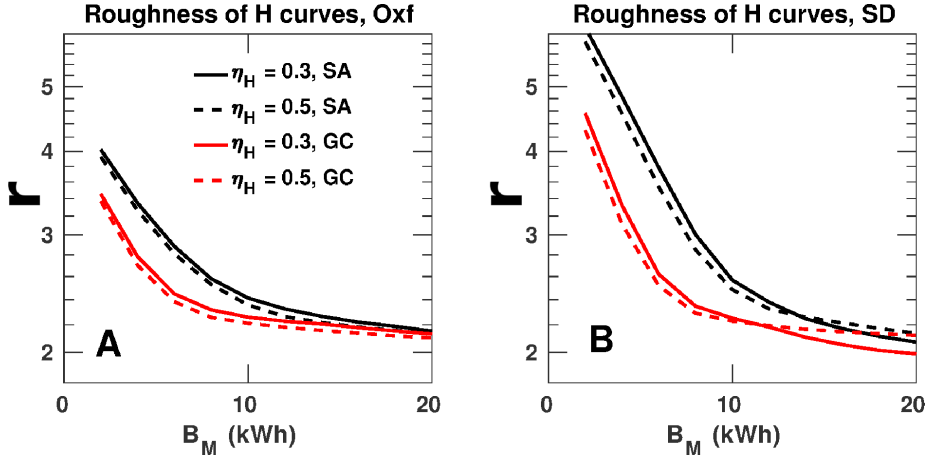

Figure 4: Systems are compared from an alternative point of view, which highlights the different usage of long-term storage when geolocation and η_H (the latter, between Panel **A** and Panel **B**) are varied: "roughness" r (Eq. 11) is depicted. Higher r values indicate higher reliance on H and a "rough" $\mathcal{H}$ profile (Fig. 5): the long-term reservoir's usage is proportionally higher on short timescales. r is inversely related to battery size, and is higher in the poleward locations. Balanced Systems with more efficient H storage rely more on it due to the smaller required PV array which, in turn, reduces the power readily available at any time.
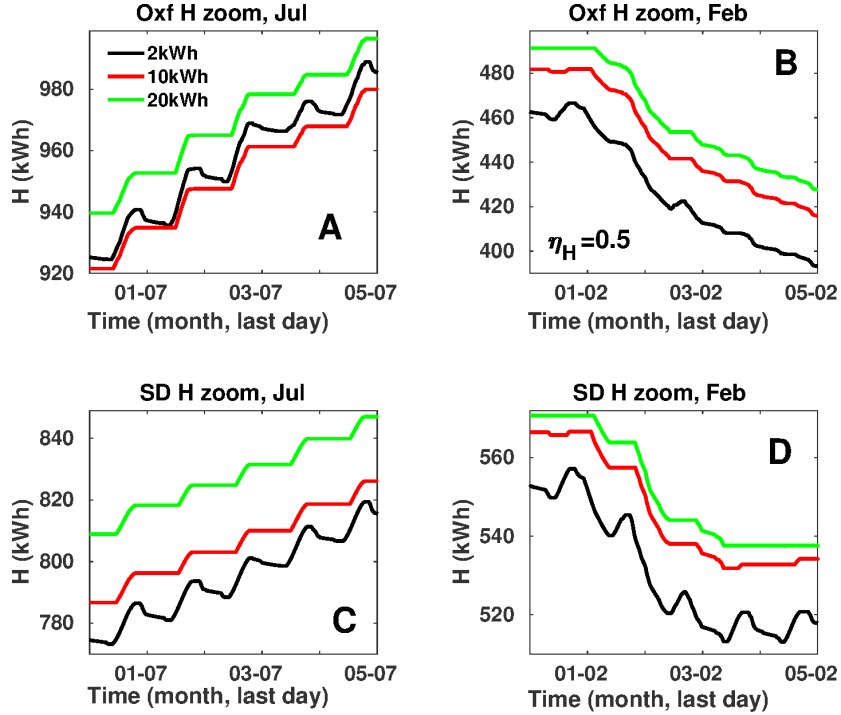
Figure 5: 5-day zooms on the curves of Fig. 4A, highlighting small-structure differences induced by battery size. A smaller B_M forces the System to "improperly" use long-term storage H for daily and sub-daily transactions. In Summer (Panels **A**,**C**), the curves are increasing on a sufficiently large timescale (> 1 day), as energy is being stored for the following Winter. Local minima (troughs) for the case of smallest battery (2 kWh) denote usage of H at short timescales. Larger batteries instead (dashed and dotted line) force H to follow a Summer "staircase pattern", with the hydrogen reservoir charging up in daylight and idling at nighttime. Pronounced local minima are also present in California in February in the small-battery case, because generation at that time of the year is already sufficient to store a significant amount energy from day to night. Legend in Panel **A** and H's efficiency refer to all plots. Figures B.9-B.12 in Appendix B display PV generation (bottom right Panels) for the initial two days of both 5-day periods.

Figure 4 depicts the "roughness" parameter, the non-dimensional number defined as

$$r \,=\, \frac{1}{H_M} \int_0^T \left| \frac{\mathrm{d}\mathcal{H}(t)}{\mathrm{d}t} \right| \, \mathrm{d}t \,, \tag{11}$$

that we introduce with the present paper to quantify the activity of H at small timescales typical of battery usage: from sub-hourly to daily. Continuous notation, instead of discrete summation, is used for generality. Sensitivity of r to battery size, hydrogen round-trip efficiency and geolocation can be inferred from Fig. 4: r combines the main three factors that determine the "amount of activity" of long-term storage H. Figure 4 also shows how roughness r is inversely proportional to η_H; while this result can be counter intuitive, it is physically jus-

tified because the System with more efficient long-term storage needs a smaller PV array, as a smaller amount of energy needs to be uploaded for winter months. This, in turn, implies that reliance on storage is on average higher on a daily basis; the fraction of energy "improperly" uploaded to/downloaded from the H reservoir at small timescales is consequently higher as well. Figure 5, by means of zooming on small-scale features of $\mathcal{H}$ curves in Winter and Summer, provides a pictorial justification for r trends. Small batteries cause the usage of H for daily storage, as the pronounced local minima of the $\mathcal{B}=2$ kWh curves suggest.

5.2. Grid-connected Systems

GC Systems' behavior is analyzed using the same model and settings used in Section 5.1: $\mathcal{B}$, $\mathcal{H}$, and X in Eqs. (6-8) are determined thirty times per geolocation combining η_H (0.3, 0.4, 0.5) with ten, evenly-spaced values of B_M from 2 to 20 kWh. Two different GC configurations are compared with the SA case. We first postulate a Grid providing a constant supply $G=G_0$ throughout the whole period, equal to 50% of the 5 MWh yearly-integrated load; this choice leaves to storage the burden of following demand. In the second case the given load is satisfied in both geolocations with the aid of a Grid that, although still providing 50% of yearly-integrated load, is freed from the constancy constraint: power provision $G=G(t)$ can oscillate randomly in time between 25% and 75% of the average demand; that is, between 143 W and 428 W. The required, simple modification to the model is the substitution $\delta \longrightarrow \delta+G$; Eq. (1) for the GC case becomes

$$\delta = X \cdot \gamma + G - \lambda;$$
(12)

The latter instance may exemplify a Grid delivering power from intermittent sources like wind farms or solar farms: domestic storage is not only used to regularize locally generated power, but to allow the distribution network to deliver variable power according to instantaneous production. Similarly to what pointed out for the SA System (Section 5.1), the modeling strategy maximizes energy efficiency and therefore minimizes PV size for the given load (and for the given Grid timeseries, in the random case). It will be shown in Section 7 that random permutations in hourly load produce undetectable changes in the ensuing System's size.

Figure 3C-D can be used to compare GC Systems to each other and with the SA systems depicted in Fig. 3A-B. An interesting conclusion is implicit in the fact that the random-supply case is virtually indistinguishable from the constant-supply one (the curve of which has therefore been omitted from the plot): the System with the 10 kWh battery is able to cope with the same effectiveness with a constant supply and with a random one. The second conclusion is that, besides obvious PV reduction, both GC Systems allow a major reduction on long-term H storage in both geolocations, as neither constant nor random supply suffer from PV's seasonal imbalance. Finally, it may be worth observing the GC System in Oxford requires a PV array approximately the same size of the San Diego's SA System for $B_M \geq 10$ (Fig. 3A and Fig. 3C,). Still, the England GC System requires significantly larger long-term storage than the California SA one in the same B_M range (Fig. 3B and Fig. 3B).

15

6. Simple CapEx analysis

The total, one-off capital cost of the System, CapEx, is examined as a function of geolocation and of $CapEx(H_M)$, the cost per kWh of H's capacity. The analysis also depends parametrically on the PV array cost per kW_p, $CapEx(kW_p)$, and on battery cost per kWh, $CapEx(B_M)$. All components' capital costs vary linearly with their size. The economical analysis is limited to CapEx because uncertainties on long-term storage's standards and future technical developments make detailed financial estimates difficult: for example, a gas storage tank may potentially last for an arbitrary long time while other components (fuel cells, electrolyzer) do not (Schmittinger and Vahidi, 2008; Carmo et al., 2013). This is analogous to the other Systems' parts, for which expenditures are however clearer to quantify: PV Systems usually require inverter replacement at approximately the modules' midlife (Colantuono et al., 2014a), while battery duration depends on frequency and depth of discharges (Divya and Østergaard, 2009).

Even if we limit the economical analysis to CapEx, H's cost remains highly uncertain: neither adequate hydrogen storage facilities have been deployed so far, particularly for domestic use, nor unified technical standards exist. This holds in general also for other potential, long-term electricity storage technologies. Economy of scale has the potential for causing a massive cost reduction, in line with what happened for decades with PV modules (Taylor et al., 2016) and batteries (Hensley et al., 2012). Cost reduction can also be achieved by means of sharing facilities across multiple homes, which could carry the additional benefit of reducing the total required capacity. The electrolysis/fuel cells cycle is chosen in this work, but other strategies are not ruled out as H storage is here defined by round-trip efficiency, η_H, and unitary cost only. Fuel cells market price is currently around 2000 \$/kW (Crow and Johnston, 2016), while electrolyzers have been reported to be around 1000 \$/kW by Penev (2013), who also estimated the reservoir's CapEx at 2.5 \$/kWh in the cheapest case (liquid hydrogen, in which case CapEx and energy expenditure for a compressor should be factored in) for large installations. 1 kW electrolyzer could suffice for coping with a load totaling 5 MWh/year; this would, however, require an extra battery to buffer the energy to be uploaded to H in instances of generation exceeding load by more than 1 kW ($\delta > 1$ kW), because **B** is full to capacity whenever H starts to be loaded. A similar mechanism would hold for fuel cells and the energy to be downloaded as soon as **B** has been depleted. The presence of such an extra battery would introduce a trade-off, with fuel cells'/electrolyzer's capacities/costs, similar to the balance analyzed in this work between PV array's size/cost and battery's size/cost.

The System capital cost is expressed by

$$\text{CapEx} = 8\,\text{kW}_p \cdot X \cdot \text{CapEx}(\text{kW}_p) + B_M \cdot \text{CapEx}(B_M) + H_M \cdot \text{CapEx}(H_M); \quad (13)$$

given the large indetermination on so many factors, we let ample variation of $CapEx(H_M)$, between 1 \$/kWh and 50 \$/kWh, with the goal of determining a

target range for it through the resulting CapEx of the whole System. The unitary cost chosen for PV arrays is $\text{CapEx}(kW_p) = 3000 \text{ \$/kW}_p$; this is multiplied by $X \cdot 8 \text{ kW}_p$ (the fraction of the 8 kW$_p$reference array) in Eq. 13. The chosen cost of batteries is 227 \$/kWh (Hensley et al., 2012). Figure 6A-B summarizes

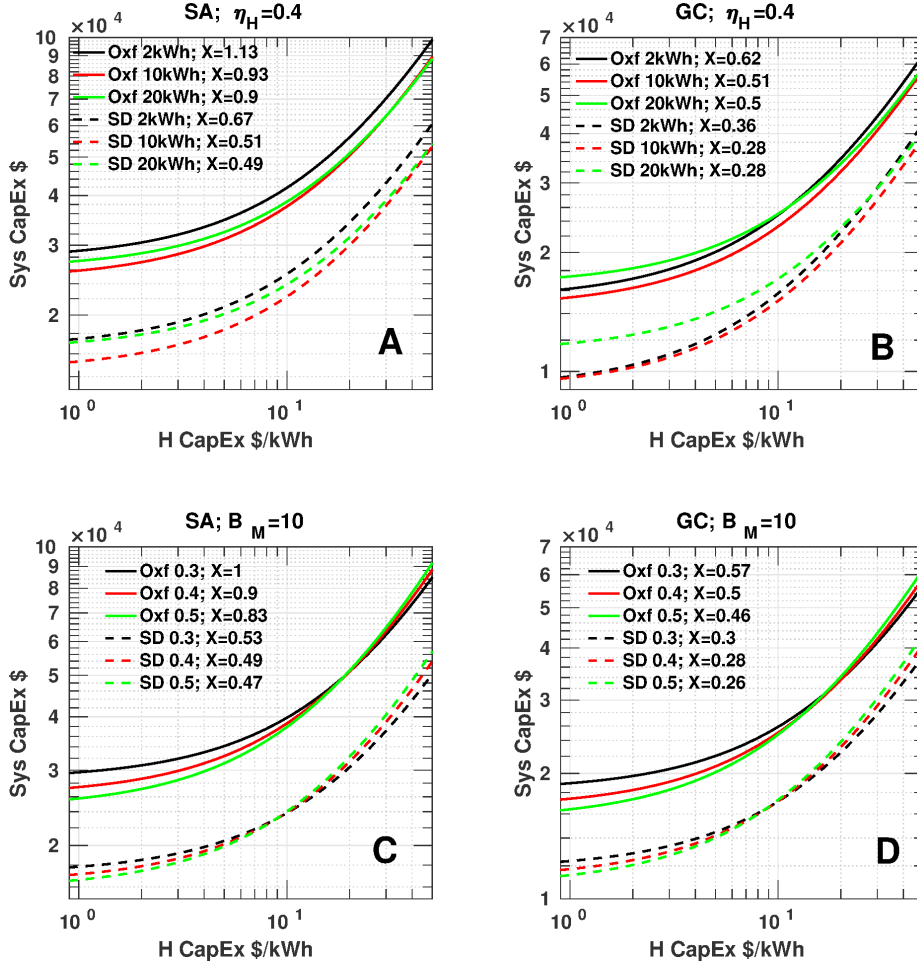
Figure 6: CapEx analysis. X represents the size of the PV array; $X = 1$ corresponds to an 8 kW$_p$ array. η_H is kept constant while battery capacity B_M varies. Geolocations are identified by line-style, battery sizes by color.

CapEx analysis for $\eta_h = 0.4$ as battery capacity varies for SA and GC Systems. The first feature to be noticed is that the curves "cluster" based on geolocations. Position on the Earth surface is the main cost discriminator because dictates PV size and seasonal capacity H_M.

The SA System with the smallest battery is always the most expensive in both locations: as seen before, a System with a small battery requires a large PV array to compensate for the increased energy penalty associated to stor-

age. The least expensive configuration is the one with the 10kWh battery for CapEx(H_M) $\leq$ 30 $/kWh in Oxford ($\mathcal{H} \leq$ 50 $/kWh in San Diego); beyond that value of CapEx(H_M), the 20 kWh battery becomes the most convenient, although at a very high System CapEx.

No detectable difference exists between the case of a constant supply fed to the System and the case of a half of such integrated supply randomly varying; each curve for GC Systems (Fig. 6B) therefore represents both instances.

Figure 6C-D reveals the influence of η_H on System's cost. The bunch of curves relative to each geolocation intersect each other for CapEx(H_M) values around 10-15 $/kWh: as determined in Section 5.1, Systems with more efficient seasonal storage require smaller PV arrays and larger seasonal capacity H_M to achieve energy balance. Therefore, they become relatively more expensive as H's cost grows and the weight of PV cost on System's price consequently decreases. This implies that, for more expensive H, the deployment of an oversized PV array, that enables H_M reduction, is convenient even if implies a generation curtailment during the sunniest season.

It may be also worth commenting on the cap that needs to be imposed on CapEx(H_M) in order to keep system's CapEx below a given threshold, say $2 \cdot 10^4$ $. Among SA Systems (Fig. 6A), all the San Diego ones can stay below the threshold, although with different maximum CapEx(H_M), which reaches 7 $/kWh in the $B_M = 10$ kWh case. On the contrary, no Oxford system is found below CapEx $= 2 \cdot 10^4$ $. This changes for Oxford GC Systems: they can stay below the $2 \cdot 10^4$ $ threshold for CapEx(H_M) as expensive as 6.5 $/kWh (15 $/kWh in San Diego). The GC cases considered here (providing 50% of the yearly load, either uniformly or with a random component) are a benchmark for the vast majority of practical cases, in which a SA system is not practical/possible.

The 2 kWh battery asks for a PV array $\sim$20% larger than what needed by the 10 kWh battery; the 1.13$\times$8 kW$_p$ array required in Oxford in the smallest battery's case (Fig.6A) corresponds to an area around 45 m^2 with current modules' conversion rate, which become more than 55 m^2 for $\eta_H = 0.3$ (corresponding to $X = 1.40$); this figure could grow larger in case of disadvantaged PV layouts, often constrained by the built environment (Colantuono et al., 2014a). The chance of reducing PV modules' area may introduce savings or prevent additional penalties not quantified in the present calculation, due to the area available to PV modules in various types of dwellings. CapEx(kW$_p$) is assumed to vary linearly with X; this assumption should be reviewed case by case depending on size and other attributes (orientation, shading, accessibility, potential rental cost) of the surface available to PV. This trade-off between battery capacity and PV array's area appears to be a key feature in densely populated areas with tall buildings.

Figure 6 hints at how expensive long-term storage would strongly impacts CapEx, particularly in the poleward location. Reasonably priced long term storage appears therefore as a key condition for making SA Systems viable or for allowing Power Grids to deliver constant or even "arbitrary" power throughout the year.

For CapEx(H_M) values within, say, 10 $/kWh, CapEx(kW$_p$) has a large rel-

ative influence on System's total CapEx. As a further test, PV cost is therefore reduced by a factor 4, from 3000 $/kW$_p$ down to 750 $/kW$_p$; this choice is also motivated by the projected reduction in PV costs predicted for the next few years (Taylor et al., 2016). Besides the prominent reduction of the overall CapEx, Systems' costs show a higher sensitivity to $\text{CapEx}(H_M)$ and $\text{CapEx}(B_M)$ than in Fig. 6; the curves cluster based on geolocations only for expensive H_M, which is also the condition that financially justifies the largest, 20 kWh battery.
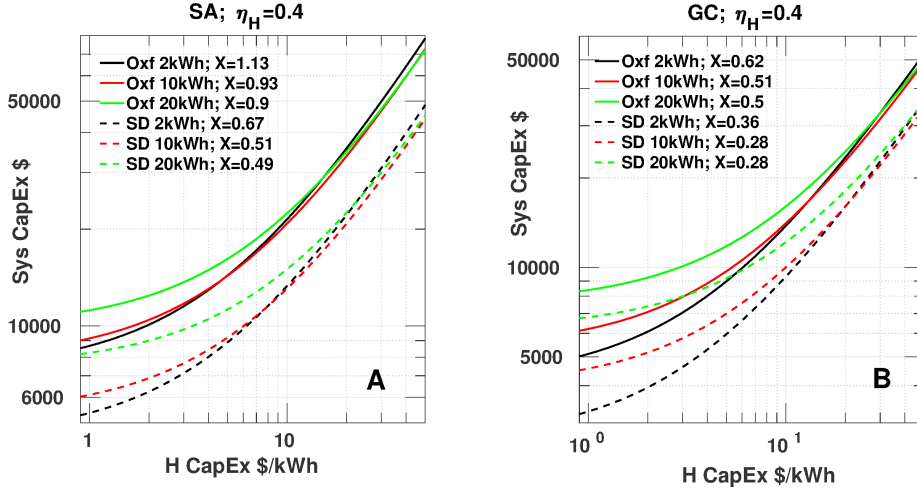

Figure 7: The same as Fig. 6 with $\text{CapEx}(kW_p) = 750$ $/kW$_p$.

7. Varying demand timeseries. Extending PV generation to multiple years. Implications for System sizing

Analyzed generation and demand timeseries are 1 year-long, mainly due to data availability. In order to generalize results, we hereby show the implications of varying λ demand timeseries and considering multiple years of PV output.

λ periodicity is 60 s; in order to test sensitivity to demand's alterations, the 365×24 hours in the 1 year time interval have been randomly permuted (without preserving the seasonal or the diurnal cycle) 120 times for various parameter combinations; in all cases, the change of PV size necessary to cope with the modified load is much smaller than 1% and within the model error, which is dictated by the 10 kWh tolerance in Eq. (9). Similarly, the behavior of $\mathcal{H}(t_n)$ (the graph of which is exemplified in Figs. 2 and 4A) remains practically unchanged after hours' permutations. Recalling the definition of δ (Table 1), random permutations in generation timeseries γ which are "reasonable" (i.e., not altering the day-night and seasonal cycle, in which case the required storage capacity could be altered) have an effect which is similar to random variations

of λ. This suggests that random generation/demand permutations do not significantly alter energy balance and System components' sizes.

Many years of PV generation need then to be considered in both geolocations, to generalize the model output and, particularly, PV array size and required H_M. Given the short length of the analyzed PV output, the authors turned their attention to GHI timeseries spanning much longer intervals. A GHI measurement station has been chosen within 100 km of the PV location in Oxford (UK Meteorological Office 2013, station ID 461, $\sim 52.23^{\circ}$N, $\sim 0.46^{\circ}$W) and San Diego (National Solar Radiation Database 2015, station ID 210008, $\sim 32.73^{\circ}$N, $\sim 117.14^{\circ}$W); timeseries are 18 year-long (1995-2012 in Oxford; 1998-2015 in San Diego) with half-hourly/hourly (Oxford/San Diego) sampling period.

The goal is to create yearly PV generation timeseries that are, from the climate and geographical standpoint, analogous to the available ones, with 60 s sampling period. Every GHI yearly record is first normalized to the available, local yearly PV generation record. Subsequently, the local sub-hourly PV variability (obtained by subtracting the local hourly means) is linearly superimposed to the normalized GHI timeseries. Finally, the 18 yearly GHI records in each location are once more individually rescaled, this time to restore the relative, year-to-year's average disparities. This way, 18 years of PV "pseudo-generation" timeseries are obtained in both locations from real GHI timeseries and used as the model input to asses the year-to-year variations in the required PV size and H's capacity (Fig. 8B,E). With the procedure just outlined, the reference year's record of PV generation used so far (in both Oxford and San Diego), integrated in time, constitutes by constructing the average of the 18 years of pseudo-generation.

Generalizing from one to many years also sheds light on the mutual relationship between PV size X and H_M: as Fig. 8B,E shows, such two variables are poorly correlated. A year associated to a PV array's required size larger than average is characterized by a relatively lower yearly irradiance per m^2, while a larger than average H_M capacity indicates reduced levels of average Winter irradiance with respect to the remainder of the year, which dictates more energy be stored in Summer. The combination of total yearly PV generation with its seasonal distribution yields the variety of cases in Fig. 8B,E. It is useful to point out that a drop in Winter generation drives a higher increase of PV size with respect to a drop of Summer yield of the same magnitude, because of the efficiency penalty affecting the energy stored from Summer to Winter. Variation of required PV size is $\sim \pm 7\%$ from average in Oxford ($\sim \pm 5\%$ in San Diego); deviations from the mean long-term storage capacity, on the contrary, are within $\sim \pm 5\%$ from average in Oxford and $\sim \pm 9\%$ in San Diego. Proportionally stronger variations of B_M in the latter location can be attributed to the much higher levels of Winter irradiance: even if year-to-year persistence of irradiance distribution is higher in California (as suggested by the larger variance associated to the first principal component, Fig. 8C,F), weather Systems there modulate an irradiance amount that is much higher in first instance. The extension to many years suggests the order of magnitude of the sizing adjust-

ments required to run the Systems over many years, which does not reach 10% for any of the 18 years in record and for any of the Systems' components.
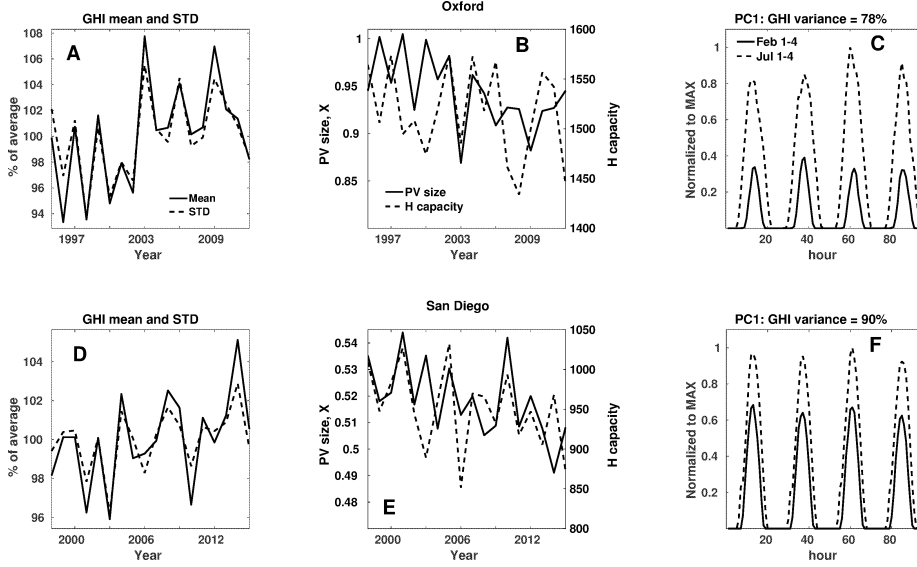

Figure 8: Panels **A,D** display GHI (kW/m^2) over the entire interval. Panels **B,E** show PV size and H capacity B_M during 18 model runs per geolocation using PV "pseudo-generation" as input, obtained from the 18-year GHI records as described in the main text. Required storage's and PV's size variability from year to year is portrayed. In Panels **C,F** the first principal component (PC1) of the 18 yearly timeseries is plotted for a few Winter and Summer days. PC1 accounts for the day-night cycle (crests and troughs with 24 hr period) and for the seasonal cycle (greater magnitude of Summer/dashed curves' peaks with respect to solid curves' peaks). PC1 is associated to 78% of variance in Oxford and to 90% of variance in San Diego; each higher order PCs explains less than 2% of variance in Oxford (less than 1% in San Diego). The significantly higher PC1's variance in Southern California can be attributed to more stable weather with respect to the British Isles. Legend in Panel **A** refers also to Panel **D**; the same holds for Panels **B** and **E** and for **C** and **F**.

Finally, as anticipated in Section 4.4, we utilize the 18-year GHI timeseries to infer which of the two PV Systems is more efficient in converting incoming radiation to electricity. As established in Appendix A (Eq. A.1), the array required in San Diego to obtain the yearly-integrated output achieved by a 1 m^2, otherwise identical array in Oxford is 0.61 m^2. This area falls down to 0.54 m^2 for GHI integrated over the 18-year record. Many factors influence conversion performance, also after having factored out arrays' technology by means of expressing sizes in kW$_\text{p}$: for example, efficiency in hotter locations is lower due to modules' overheating. Factoring out orientation is also subtle, particularly when comparing arrays at widely different latitudes: elevation angle can be optimized in more than one way, depending on whether maximal yearly generation is sought or intraseasonal balance is privileged instead. Moreover, orientation is rarely optimal for real, domestic PV arrays (usually constrained by the existing built environment, Colantuono et al. 2014a) and often known/reported by the

owner with significant approximation (*ibid.*). This said, San Diego's array looks somehow disadvantaged in this case study, due to reported azimuth and partial shading (Appendix A).

8. Discussion and Conclusions

PV arrays, combined with a set of battery-hydrogen hybrid systems (BHHS) storage solutions of varying sizes, efficiencies and unitary capital costs (CapEx), are required to satisfy the same, 1-year domestic demand in two different geolocations: Oxford, UK, and San Diego, California, which mutually widely differ in latitude ($\sim 20^\mathrm{o}$) and climate. The model minimizes energy use: power can be uploaded to/drawn from the least efficient reservoir (mimicking a hydrogen tank, H, coupled to an electrolyzer-fuel cell cycle) only when the most efficient one (battery **B**, with an efficiency value $\eta_B = 0.85$ compatible with lithium-ion batteries' current performance) is full/empty; this rule maximizes the usage of the most efficient storage option within the given constraints (balance between yearly generation and consumption, and minimization of PV array size). The levels of both reservoirs as function of time are output by the model; PV array size and H capacity H_M in both locations are being sized dynamically as function of local generation per m^2, battery size and H's efficiency η_H.

The environmental factors determining performance of BHHSs coupled to PV have not received adequate attention so far in literature. The prevailing focus is on finding optimal dispatching rules to optimize some functions of financial variables. This approach, while certainly useful, rarely, if ever, considers the effect, on storage size and charge states, due to the variability of irradiance in space (across the Earth surface) and time (over many years).

The English location requires, as expected, a much bigger ($\sim$170% or more, depending on parameters) PV array. It also requires an analogously larger H_M, due to bigger seasonal differences in irradiance: more energy needs to be stored during Summer months for Winter usage. The ratio of Oxford's vs San Diego's PV size is larger than the ratio of San Diego's vs Oxford's yearly-integrated generation per m^2, due to the prominent energy penalty imposed by H storage.

The penalty imposed by a small battery, with the ensuing reliance on H for short timescales, is proportionally higher in the equatorward location, where a significant amount of energy can be carried from day to night also during Winter. San Diego's array becomes even smaller (by 11%, like its cost) relatively to Oxford if generation is scaled to local GHI. This is partially justified as San Diego array appears to be less optimized than Oxford's one. On the other hand, the worse conversion efficiency in the hottest location can partially explain the extant efficiency gap. Position on the Earth surface is the main cost discriminator because dictates PV size and seasonal capacity H_M.

In a second modeling effort a grid is considered, which supplies 50% of the integrated yearly load. In the first case, supply is constant, meaning neither demand is followed nor Grid intake can be reduced: the user is required to store the Grid's provision during times of lower demand. The second case allows more freedom to the Grid which, with respect to the yearly-integrated demand,

supplies 25% of constant power and 25% of randomly fluctuating power. These Grid-connected (GC) cases are virtually identical one to each other in terms of PV and storage sizing and of the reservoirs' states of charge; required PV size shrinks to ∼55%-60% of the corresponding SA's size.

Increasing battery size beyond ∼10 kWh does not decrease significantly either required PV size or H_M; this holds for both SA and GC cases. 10 kWh is of the same order of magnitude of the average daily energy usage, ∼14 kWh, corresponding to 5 MWh yearly-integrated value. On the contrary, a very small battery (2 kWh) requires a noticeably larger PV array, as inefficient long-term storage is "improperly" used on a daily/hourly basis. In this respect, a simple metrics has been defined: roughness $r = H_M^{-1} \int_0^T |\,\mathrm{d}\mathcal{H}/\,\mathrm{d}t|\,\mathrm{d}t$ quantifies the amount of activity of long-term storage. High r values denote frequent charging-discharging cycles. Low values indicate instead the "appropriate" use of long-term storage: bringing power from Summer to Winter. r decreases with increasing battery capacity, decreasing $\eta_{_H}$ values and decreasing latitude.

The required H_M value for $\mathcal{B} = 10$ kWh and $\eta_{_H} = 0.4$ is ∼1230 kWh in Oxford (PV array size being 93% of the local reference 8 kW$_\mathrm{p}$ System) and ∼750 kWh in San Diego (PV size 51%) for the SA System and, respectively, ∼830 kWh (PV 51%) and ∼600 kWh (28%) for GC Systems.

The global minimum for PV array size is attained if the entire storage capacity is of battery type, a configuration maximizing round-trip efficiency and therefore minimizing the yearly-integrated energy required to satisfy demand. It is actually the higher cost of efficient storage that suggests a multiple scale solution; a huge battery, of the order of 1 MWh, is presently not a realistic proposal for SA Systems. To identify financially-plausible components' combinations, a simple CapEx function has been formulated. Reference costs of 3000 $/kW$_\mathrm{p}$ (later reduced to 750 $/kW$_\mathrm{p}$, to model plausible CapEx few years from now) and 227 $/kWh are assumed for PV modules and batteries, respectively, letting H cost CapEx(H_M) vary between 1 and 50 $/kWh. Geolocation is the main physical factor in determining System's cost differences, as it is the main drive of seasonal storage capacity H_M (a consequence of variability of irradiance over the year) and of PV size.

For a given location, the trade-off between PV size and B_M appears as a key feature of Systems with long-term storage that are either standalone or partially fulfilled by a Grid providing power unrelated to demand. With the specified cost for PV and batteries, a CapEx not higher than $2 \cdot 10^4$ $ is attainable for CapEx(H_M) as high as 7 $/kWh by standalone Systems in San Diego. In Oxford, on the contrary, only grid-connected Systems can meet the $2 \cdot 10^4$ $ cap, for a CapEx(H_M) of 6 $/kWh (18 $/kWh for a GC System in San Diego) in the most favorable condition among those analyzed. Considering "cost" in a wider sense, for example factoring in the larger area taken up by the PV array required by a System endowed with a small battery, may increase the benefit of deploying a larger short-term storage capacity B_M.

Randomly permuting hours of the demand timeseries does not affect System's sizing and behavior. Considering many years of generation causes changes

in PV array size and B_M that are, in all conditions, less than 10% of the reference year's values. PV size variations are higher in Oxford ($\sim \pm 7\%$ vs $\sim \pm 5\%$ in San Diego), while deviations from the mean long-term storage capacity are lower there ($\sim \pm 5\%$ vs $\sim \pm 9\%$ in San Diego): stronger Winter insolation makes the equatorward location more sensitive to weather patterns than the poleward one, in spite of a reduced variability of weather/irradiance.

References

Aghaei, J. and Alizadeh, M.-I. (2013). Demand response in smart electricity grids equipped with renewable energy sources: A review. *Renewable and Sustainable Energy Reviews*, 18:64–72.

Beaudin, M., Zareipour, H., Schellenberglabe, A., and Rosehart, W. (2010). Energy storage for mitigating the variability of renewable electricity sources: An updated review. *Energy for Sustainable Development*, 14(4):302 – 314.

Bigdeli, N. (2015). Optimal management of hybrid pv/fuel cell/battery power system: A comparison of optimal hybrid approaches. *Renewable and Sustainable Energy Reviews*, 42:377 – 393.

Boyle, G. (2012). *Renewable electricity and the grid: the challenge of variability.* Earthscan.

Brinkhaus, M., Jarosch, D., and Kapischke, J. (2011). All year power supply with off-grid photovoltaic system and clean seasonal power storage. *Solar Energy*, 85(10):2488 – 2496.

Carmo, M., Fritz, D. L., Mergel, J., and Stolten, D. (2013). A comprehensive review on pem water electrolysis. *International journal of hydrogen energy*, 38(12):4901–4934.

Cau, G., Cocco, D., Petrollese, M., Kær, S. K., and Milan, C. (2014). Energy management strategy based on short-term generation scheduling for a renewable microgrid using a hydrogen storage system. *Energy Conversion and Management*, 87:820–831.

Cebulla, F., Naegler, T., and Pohl, M. (2017). Electrical energy storage in highly renewable european energy systems: Capacity requirements, spatial distribution, and storage dispatch. *Journal of Energy Storage*, 14:211 – 223.

Celik, A. N. (2007). Effect of different load profiles on the loss-of-load probability of stand-alone photovoltaic systems. *Renewable Energy*, 32(12):2096–2115.

Colantuono, G., Everard, A., Hall, L. M., and Buckley, A. R. (2014a). Monitoring nationwide ensembles of pv generators: Limitations and uncertainties. the case of the uk. *Solar Energy*, 108:252 – 263.

Colantuono, G., Wang, Y., Hanna, E., and Erdélyi, R. (2014b). Signature of the north atlantic oscillation on british solar radiation availability and pv potential: The winter zonal seesaw. *Solar Energy*, 107:210–219.

Correia, J., Bastos, A., Brito, M., and Trigo, R. (2017). The influence of the main large-scale circulation patterns on wind power production in portugal. *Renewable Energy*, 102:214–223.

Crow, M. and Johnston, R. (2016). Ceres Power Holding. A fuel cell in every home and business. Technical report, Edison Investment Research Limited.

Denholm, P., O'Connell, M., Brinkman, G., and Jorgenson, J. (2015). Overgeneration from solar energy in california. a field guide to the duck chart. Technical report, National Renewable Energy Lab.(NREL), Golden, CO (United States).

Divya, K. and Østergaard, J. (2009). Battery energy storage technology for power systemsan overview. *Electric Power Systems Research*, 79(4):511–520.

Emeis, S. (2012). *Wind energy meteorology: atmospheric physics for wind power generation*. Springer Science & Business Media.

Energy Efficiency Indicators (2016). World Energy Council. https://www.wec-indicators.enerdata.eu/household-electricity-use.html.

Gabrielli, P., Gazzani, M., Martelli, E., and Mazzotti, M. (2017). Optimal design of multi-energy systems with seasonal storage. *Applied Energy*.

Gholz, H. L., Wedin, D. A., Smitherman, S. M., Harmon, M. E., and Parton, W. J. (2000). Long-term dynamics of pine and hardwood litter in contrasting environments: toward a global model of decomposition. *Global Change Biology*, 6(7):751–765.

Glavin, M., Chan, P. K., Armstrong, S., and Hurley, W. (2008). A stand-alone photovoltaic supercapacitor battery hybrid energy storage system. In *Power Electronics and Motion Control Conference, 2008. EPE-PEMC 2008. 13th*, pages 1688–1695. IEEE.

Gomez, G., Martinez, G., Galvez, J. L., Gila, R., Cuevas, R., Maellas, J., and Bueno, E. (2009). Optimization of the photovoltaic-hydrogen supply system of a stand-alone remote-telecom application. *International Journal of Hydrogen Energy*, 34(13):5304 – 5310.

Hensley, R., Newman, J., and Rogers, M. (2012). Battery technology charges ahead. *McKinsey Quarterly*, 3:5–50.

International Renewable Energy Agency (2015). Renewable Power Costs Plummet: Many Sources Now Cheaper than Fossil Fuels Worldwide. Available at https://pvoutput.org/display.jsp?sid=25601.

Jacob, A. S., Banerjee, R., and Ghosh, P. C. (2018). Sizing of hybrid energy storage system for a pv based microgrid through design space approach. *Applied Energy*, 212:640 – 653.

Jallouli, R. and Krichen, L. (2012). Sizing, techno-economic and generation management analysis of a stand alone photovoltaic power unit including storage devices. *Energy*, 40(1):196 – 209.

Juul, N. (2012). Battery prices and capacity sensitivity: Electric drive vehicles. *Energy*, 47(1):403–410.

Klein, S. and Beckman, W. (1987). Loss-of-load probabilities for stand-alone photovoltaic systems. *Solar Energy*, 39(6):499–512.

Kleissl, J. (2013). *Solar energy forecasting and resource assessment*. Academic Press.

Kolhe, M., Agbossou, K., Hamelin, J., and Bose, T. (2003). Analytical model for predicting the performance of photovoltaic array coupled with a wind turbine in a stand-alone renewable energy system based on hydrogen. *Renewable Energy*, 28(5):727 – 742.

Lacko, R., Drobnic, B., Sekavcnik, M., and Mori, M. (2014). Hydrogen energy system with renewables for isolated households: The optimal system design, numerical analysis and experimental evaluation. *Energy and Buildings*, 80:106 – 113.

Lam, J. C., Wan, K. K., Tsang, C., and Yang, L. (2008). Building energy efficiency in different climates. *Energy Conversion and Management*, 49(8):2354 – 2366.

Li, C.-H., Zhu, X.-J., Cao, G.-Y., Sui, S., and Hu, M.-R. (2009). Dynamic modeling and sizing optimization of stand-alone photovoltaic power systems using hybrid energy storage technology. *Renewable Energy*, 34(3):815 – 826.

Lichman, M. (2013). UCI machine learning repository.

Luo, X., Wang, J., Dooner, M., and Clarke, J. (2015). Overview of current development in electrical energy storage technologies and the application potential in power system operation. *Applied Energy*, 137:511 – 536.

Maclay, J. D., Brouwer, J., and Samuelsen, G. S. (2007). Dynamic modeling of hybrid energy storage systems coupled to photovoltaic generation in residential applications. *Journal of Power Sources*, 163(2):916 – 925. Selected Papers presented at the FUEL PROCESSING FOR HYDROGEN PRODUCTION SYMPOSIUM at the 230th American Chemical SocietyNational Meeting Washington, DC, USA, 28 August 1 September 2005.

Marchenko, O. and Solomin, S. (2017). Modeling of hydrogen and electrical energy storages in wind/pv energy system on the lake baikal coast. *International Journal of Hydrogen Energy*, 42(15):9361 – 9370.

Moshövel, J., Kairies, K.-P., Magnor, D., Leuthold, M., Bost, M., Gährs, S., Szczechowicz, E., Cramer, M., and Sauer, D. U. (2015). Analysis of the maximal possible grid relief from pv-peak-power impacts by using storage systems for increased self-consumption. *Applied Energy*, 137:567–575.

Mulder, G., Six, D., Claessens, B., Broes, T., Omar, N., and Van Mierlo, J. (2013). The dimensioning of pv-battery systems depending on the incentive and selling price conditions. *Applied Energy*, 111:1126–1135.

National Solar Radiation Database (2015). https://nsrdb.nrel.gov/. Accessed: 2017-07-31.

Olsson, L. E. (1994). Energy-meteorology: a new discipline. *Renewable energy*, 5(5-8):1243–1246.

Oxford PV array (2016). https://shkspr.mobi/blog/2014/12/a-year-of-solar-panels-open-data/.

Penev, M. R. (2013). Hydrogen for Energy Storage https://www.h2fcsupergen.com/wp-content/uploads/2013/06/Hybrid-Hydrogen-Energy-Storage-Michael-Penev-National-Energy-Research-Laboratory.pdf.

Prasad, A. A., Taylor, R. A., and Kay, M. (2015). Assessment of direct normal irradiance and cloud connections using satellite data over australia. *Applied Energy*, 143:301–311.

PVOutput.org (2017a). https://pvoutput.org.

PVOutput.org (2017b). https://pvoutput.org/display.jsp?sid=25601. San Diego timeseries.

PVOutput.org (2017c). https://pvoutput.org/display.jsp?sid=25687. Oxford timeseries.

Qi, Z. (2013). *Proton Exchange Membrane Fuel Cells*. CRC Press.

Rastler, D. (2010). *Electricity energy storage technology options: a white paper primer on applications, costs and benefits*. Electric Power Research Institute.

Rotter, R. P., Palosuo, T., Kersebaum, K. C., Angulo, C., Bindi, M., Ewert, F., Ferrise, R., Hlavinka, P., Moriondo, M., Nendel, C., Olesen, J. E., Patil, R. H., Ruget, F., and Takac, J. (2012). Simulation of spring barley yield in different climatic zones of northern and central europe: A comparison of nine crop models. *Field Crops Research*, 133:23 – 36.

Running, S. W. and Nemani, R. R. (1988). Relating seasonal patterns of the avhrr vegetation index to simulated photosynthesis and transpiration of forests in different climates. *Remote Sensing of Environment*, 24(2):347 – 367.

Scamman, D., Newborough, M., and Bustamante, H. (2015). Hybrid hydrogen-battery systems for renewable off-grid telecom power. *International Journal of Hydrogen Energy*, 40(40):13876 – 13887.

Schenk, K., Misra, R., Vassos, S., and Wen, W. (1984). A new method for the evaluation of expected energy generation and loss of load probability. *IEEE transactions on power apparatus and systems*, 103(2):294–303.

Schmittinger, W. and Vahidi, A. (2008). A review of the main parameters influencing long-term performance and durability of PEM fuel cells. *Journal of power sources*, 180(1):1–14.

Steinke, F., Wolfrum, P., and Hoffmann, C. (2013). Grid vs. storage in a 100% renewable europe. *Renewable Energy*, 50:826–832.

Taylor, M., Ralon, P., and Ilas, A. (2016). The power to change: solar and wind cost reduction potential to 2025. Technical report, International Renewable Energy Agency (IRENA).

Tesfahunegn, S., Ulleberg, Ø., Vie, P., and Undeland, T. (2011). Optimal shifting of photovoltaic and load fluctuations from fuel cell and electrolyzer to lead acid battery in a photovoltaic/hydrogen standalone power system for improved performance and life time. *Journal of Power Sources*, 196(23):10401 – 10414.

UK Meteorological Office (2013). Met Office Integrated Data Archive System (MIDAS) Land and Marine Surface Stations Data (1853-current), [internet].NCAS British Atmospheric Data Centre, 2013. Available from http://badc.nerc.ac.uk/view/badc.nerc.ac.uk__ATOM__dataent_ukmo-midas.

Ulleberg, O. (2004). The importance of control strategies in pv-hydrogen systems. *Solar Energy*, 76(1):323 – 329.

Zhang, Y., Campana, P. E., Lundblad, A., and Yan, J. (2017). Comparative study of hydrogen storage and battery storage in grid connected photovoltaic system: Storage sizing and rule-based operation. *Applied Energy*, 201:397 – 411.

Zhou, H., Bhattacharya, T., Tran, D., Siew, T. S. T., and Khambadkone, A. M. (2011). Composite energy storage system involving battery and ultracapacitor with dynamic energy management in microgrid applications. *IEEE transactions on power electronics*, 26(3):923–930.

Zhou, K., Ferreira, J., and de Haan, S. (2008). Optimal energy management strategy and system sizing method for stand-alone photovoltaic-hydrogen systems. *International Journal of Hydrogen Energy*, 33(2):477 – 489.

Appendix A. Load and generation timeseries

The domestic electricity consumption timeseries, downloaded from Lichman (2013), consist of about 4 years of power demand sampled every 60 s, between 2006 and 2010; year 2007 has been picked to minimize gaps. The household is located in France and is relatively substantial (includes a tumble dryer and an air conditioner), but does use gas for cooking and space heating; the latter detail is relevant as electric heating would have introduced a prominent dependency on local climate that would have made questionable the usage of such a load in an environment like San Diego, characterized by an arid climate and a significantly lower latitude.

Power generation data in Oxford ($\sim 52^{\text{o}}$N) has been downloaded from the web-site of a PV enthusiast who kindly makes the 2014 timeseries of his domestic System publicly available (Oxford PV array, 2016). The azimuth angle is quantified as few degrees west of South, and its elevation matches the roof at about 45°. The sampling period is 60 s, as for the demand timeseries; data from the same System is also available on PVOutput.org (2017c), but with longer (300 s) sampling period. In case of gaps of 1 day or more, in this timeseries and the others, the main strategy adopted is to replace missing strings with values that are symmetrical in time with respect to the closest solstice/equinox to minimize seasonality-induced error. In case of gaps of few hours, missing strings are replaced with values from the previous/next day; gaps few minutes long have been instead filled by interpolating between nearby values. The Oxford timeseries actually runs from late December 2013 to late December 2014; the initial days of the sequence have been moved to the bottom to obtain an yearly timeseries. The size of the Oxford array is 4 kW_p; its generation is multiplied by 2 to obtain the Oxford reference load used here, in order to better approximate the magnitude of the demand; the ensuing 8 kW_p PV array is roughly equivalent to an area of 40 m^2, depending on technology. The precise array size that satisfies the model's equations is attained case by case and expressed by the scaling factor X.

San Diego ($\sim 33^{\text{o}}$N) generation data has been obtained from PVOutput.org (2017b); it's tilt is 22.5^{o} and its azimuth angle is specified as "southwest". Some shading is reported for the San Diego System, while it is absent from Oxford's one. San Diego System is larger (7.8 kW_p); however, its size is not of primary interest here as its output is normalized to the Oxford, 8 kW_p array's yearly-integrated generation: the ratio

$$x = \frac{\text{Oxford System yearly generation per } \text{kW}_\text{p}}{\text{San Diego System yearly generation per } \text{kW}_\text{p}} = 0.61 \,, \qquad \text{(A.1)}$$

tells that an array of $0.61 \times 8\text{KW}_\text{p} = 4.88\text{KW}_\text{p}$ is the needed installation to achieve in San Diego the same output achieved by the 8KW_p Oxford's array for the used 1-year timeseries. The fraction X in the main text (e.g. Fig. 2) implicitly includes this scaling factor when referred to the size of the San Diego System.

29

Appendix A.1. Resolution

The San Diego timeseries' sampling period is 300 s, as usual on PVOutput.org (2017a); data have been interpolated to match the 60 s-resolution of both demand (Lichman, 2013) and Oxford PV array (2016). Increasing sampling rate by interpolation could create the illusion of a battery charge state $\mathcal{B}(t_n)$ smoother than the actual one. To bring an argument against this chance, we apply the definition of roughness (Eq. 11; the normalizing factor is omitted as is the same, total generation, in both cases) to both the available Oxford PV generation timeseries (Oxford PV array 2016, with a 60 s sampling period, and PVOutput.org 2017c, with a 300 s period):

$$r_i = \int_0^T \left| \frac{\mathrm{d}\gamma_{O,i}(t)}{\mathrm{d}t} \right| \mathrm{d}t \,, \tag{A.2}$$

where γ_O represents generation in Oxford and indices denote the sampling period in seconds. We obtain

$$1 - r_{300}/r_{60} < 1\% \,, \tag{A.3}$$

indicating that timeseries with either 60 s or 300 s resolution produce the same model outcome in Oxford. This should be even more the case in San Diego, given the smoother behavior of irradiance in time.

Appendix B. Samples of model runs and generation

Charts in this Section display, as an example of model's inner working mode, the seven variables on the left-hand sides of Eqs. (1-7) and PV generation in the SA case. Winter and Summer days are examined in Oxford and San Diego, with different battery sizes, to provide clues on System's behavior as parameters, geolocation and climatic conditions change. Figure B.9 shows model's variables in Oxford on two successive Winter days. On both days, generation is sufficient to upload some energy to the 4 kWh battery (as proved by the u^B panel). Due to its relatively small size, **B** saturates before noon (**B** panel) causing excess power being uploaded to H instead (u^H panel). On the second day, sunlight is weaker and the power uploaded to **B** is consequently smaller; the battery does not saturate and u^H is identically zero.

At the end of the 48 hour period, state of charge $\mathcal{H}$ is lower than at the beginning; power downloaded from H exceeds uploaded one, as to be expected given the season. The situation is opposite if two Summer days are considered (Fig. B.10), with $\mathcal{H}$ level increased at the end of the 48 hour interval; d^H is identically zero while u^H is positive during the day, in spite of the larger battery (20 kWh) considered in this case.

In San Diego (Figs. B.11-B.12) the higher irradiance is offset by the consequently smaller size of the PV array required to meet demand; Summer-Winter imbalance is greatly reduced, like the weather modulation to the irradiance curves ("PV" subplots in Figs. B.11-B.12).
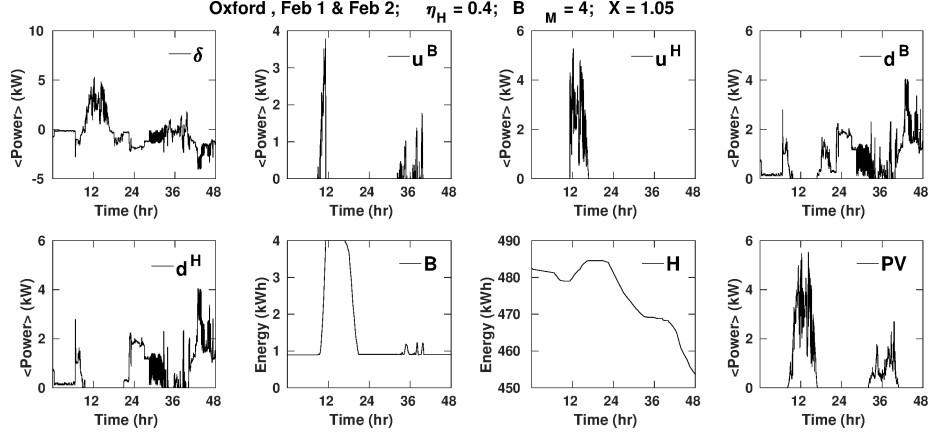
Figure B.9: System's operations are investigated in Oxford during two Winter days (reported on chart's title together with H's efficiency, battery capacity, and PV size as fraction of the reference 8 kW$_p$ array). The variables defined by Eqs. (1-7) are plotted, from left to right and top to bottom; the last (bottom-right) panel depicts PV generation. The 48 hours interval starts at 00:01 on the first day and ends at 24:00 on the second day. The <kW> label indicates power in kW averaged over every 60 s sampling interval. Power's sign is positive when uploaded to reservoirs and negative when downloaded from them. d^H, which is downloaded from H to be formally uploaded to $\mathbf{B}$, is endowed with positive sign. As discussed in the main text, d^H does not undergo the energy penalty associated to battery upload in Eq. (6): even if $d^H > 0$ is indeed triggered by $\mathcal{B} < B_m$, d^H helps meeting demand without transiting through battery.
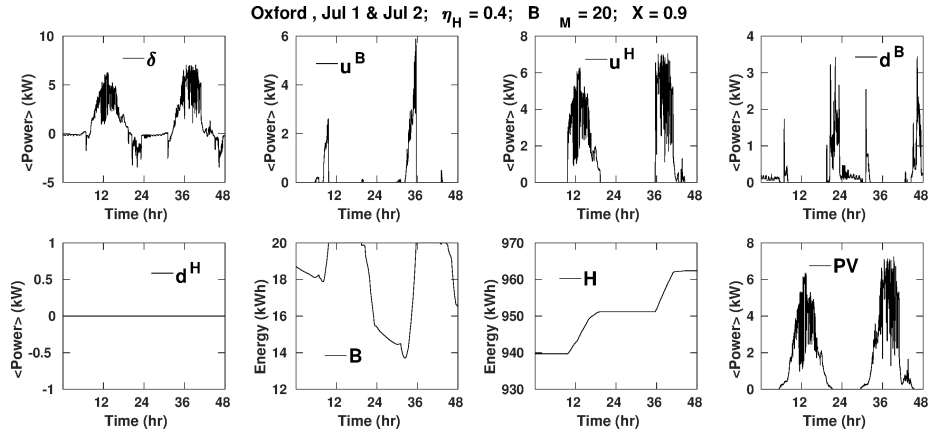

Figure B.10: Same as Fig. B.9, except that the 48 hour sampled interval belongs to July; battery capacity is 20 kWh.
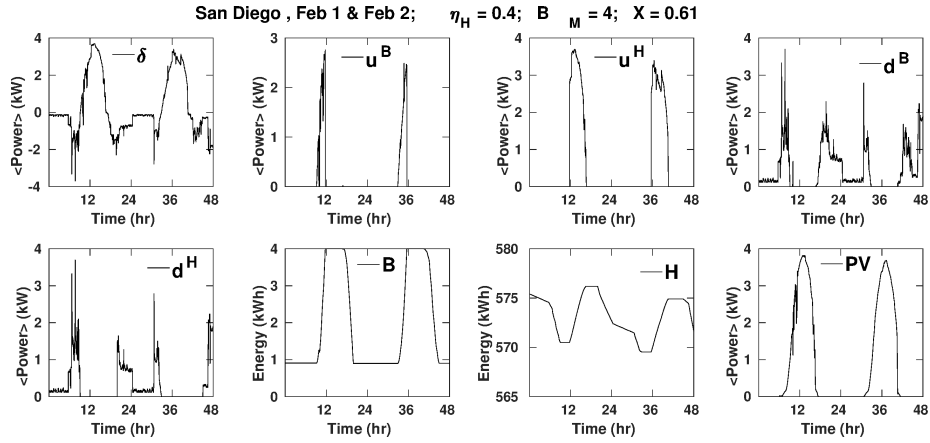
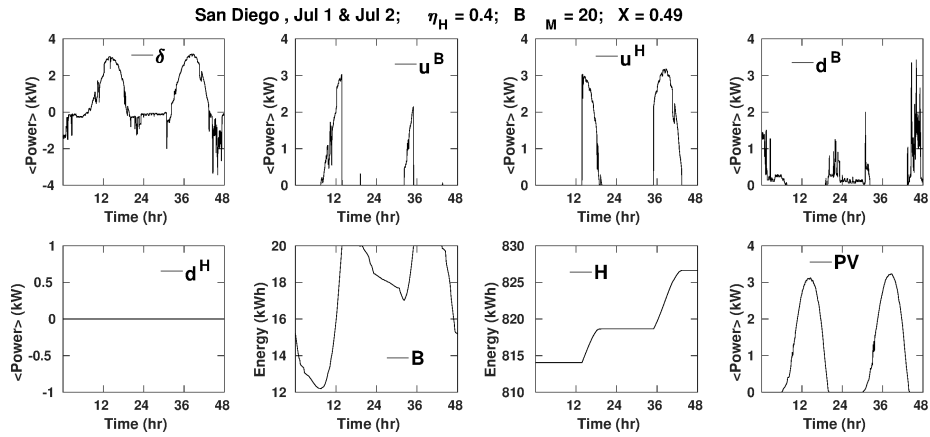Figure B.11: Equivalent to Fig. B.9 for the San Diego System.

Figure B.12: Equivalent to Fig. B.10 for the San Diego System.

Appendix C. Alternative formulation for Eqs. (2-5)

The Heaviside's Function formalism used in Eqs. (2-5) is concise and with the practical advantage of expressing the problem in terms of mathematical functions only. Such a formulation is the one used for the actual model's code (in Matlab/Octave). An alternative formulation of Eqs. (2-5) in terms of **if** conditions is provided below.

Equation (2) defines the power uploaded to battery. Remembering that δ, the difference between generation and demand, is defined by Eq. (1), Eq. (2) can be written

if $\delta > 0$ **then**
    if $B_M \geq \eta_B \delta + \mathcal{B}(t_{n-1})$ **then**
        $u^B = \delta$
    else if $B_M < \eta_B \delta + \mathcal{B}(t_{n-1})$ **then**
        $u^B = \left[B_M - \mathcal{B}(t_{n-1})\right]/\eta_B$
    end if
else
    $u^B = 0$
end if

The second term of Eq. (2) does not include the condition ensuring $\delta > 0$: the latter is implied by $B_M < \eta_B \delta + \mathcal{B}(t_{n-1})$ which, in turn descends from being $B_M \geq \mathcal{B}(t_{n-1})$; this consideration hods also for following Eq. (3), which can be written

if $\delta > 0$ **and** $B_M < \eta_B \delta + \mathcal{B}(t_{n-1})$ **then**
    $u^H = \delta + \left[\mathcal{B}(t_{n-1}) - B_M\right]/\eta_B$
else
    $u^H = 0$
end if

Equation (3) routes to seasonal storage the quantity δ diminished by the fraction (if any) of δ that fills the battery.

Equation (4) can be written

if $\delta < 0$ **then**
    $d^B = -\delta$
else
    $d^B = 0$
end if

Equation (5) can be written

if $\delta < 0$ **and** $\mathcal{B}(t_{n-1}) < B_m$ **then**
    $d^H = -\delta$
else
    $d^H = 0.$
end if